

ELECTROMAGNETIC WAVE PROPAGATION IN OMEGA WAVEGUIDES: DISCRETE COMPLEX MODES AND APPLICATION TO A RIDGE WAVEGUIDE

A. L. Topa, C. R. Paiva, and A. M. Barbosa

Instituto de Telecomunicações
Department of Electrical and Computer Engineering
Instituto Superior Técnico
Technical University of Lisbon
Av. Rovisco Pais 1, 1049-001 Lisboa, Portugal

Abstract—This paper addresses guided wave propagation in three-dimensional open omega waveguides. The analysis uses a mode matching technique, is focused on the discrete modes and includes both guidance and leakage behavior. It is shown that, in some ranges of operation, the discrete surface modes turn into leaky modes due to TE-TM mode coupling, an effect already known for isotropic dielectric waveguides. The numerical results show the influence of the medium and geometrical parameters on the attenuation and phase constants of these leaky modes.

1 Introduction

2 Grounded Omega Slab with Upper-Shielding

2.1 Omega Media

2.2 Field Theory and Modal Equations

3 Omega Ridge Waveguide

3.1 Analysis of the Step Discontinuity

3.2 Modal Equation of the 3D Waveguide

4 Numerical Results

5 Conclusion

Acknowledgment

References

1. INTRODUCTION

The pseudochiral or omega medium has been presented for the first time in 1992, by Saadoun and Engheta [1]. This medium can be obtained by doping a host dielectric medium with omega shaped conducting inclusions, where the electric and magnetic fields induce both electric and magnetic polarizations. However, unlike chiral media [2], electric and magnetic polarizations are perpendicular to each other. Therefore omega media are nonchiral.

This medium has received considerable attention from the electromagnetics research community. New results have been presented in the literature concerning the analysis of reflection and transmission properties of planar arrays of omega particles [3] and planar structures of uniaxial chiro-omega slabs [4, 5], radiation of elementary sources embedded in omega media [6], extraction of constitutive parameters of omega materials [7, 8], wave propagation in closed parallel plate [9], circular [10] and rectangular waveguides partially [11, 12] or totally filled [13] with omega media and in a NRD waveguide with an omega slab [14].

The analysis of wave propagation in open structures with omega media has been limited to two-dimensional (2D) slab structures [15–18]. In the present paper, results for electromagnetic wave propagation in three-dimensional (3D) omega waveguides are presented, as far as the authors are aware, for the first time, expanding preliminary results presented in [19]. The analysis is applicable to different types of 3D rectangular open waveguides and is applied to the omega ridge waveguide depicted in Fig. 1. Attention is focused not only on the guiding properties but also on leakage effects: it is shown that in some ranges of operation, leakage will occur in the form of a lateral exiting wave. Therefore results are derived for the phase and attenuation constants of the complex modes propagating in the structure.

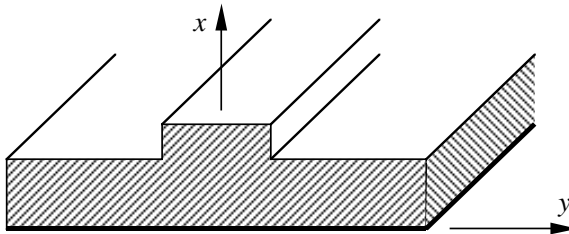


Figure 1. Omega ridge waveguide.

In a 3D waveguide like this one, propagating surface waves bounce back and forth horizontally in the inner region undergoing total or partial reflection after each bounce. Therefore, the analysis requires the characterization of step discontinuities. A rigorous analysis of a step discontinuity in an open waveguide is a difficult problem since the fields must be expressed not only in terms of discrete modes but also in terms of the continuous spectrum of radiation modes [20]. In the present work, the analysis is focused only on the discrete modes and is done by a generalization of the Peng and Oliner's method [21, 22]. In this method, the structure is covered by an upper-shielding consisting of a perfectly conducting plane. If the shielding is sufficiently far from the waveguide the discrete slow modes remain considerably unperturbed and the results are very similar to those obtained for the fully open waveguide.

The remaining sections of this paper are organized as follows: Section 2 contains a brief reference to omega media and a preliminary analysis of 2D planar shielded omega waveguides since these are the constituent blocks of the 3D waveguide inner and outer regions. In Section 3 the 3D omega ridge waveguide is analyzed starting with the characterization of the step discontinuity and applying a mode matching technique and the transverse resonance method. In Section 4 numerical results are presented including the operational diagrams as well as the phase and attenuation constants for the first leaky modes. Finally, in Section 5, a few concluding remarks are drawn.

2. GROUNDED OMEGA SLAB WITH UPPER-SHIELDING

2.1. Omega Media

Omega media belong to the general class of reciprocal bianisotropic media [23], whose constitutive relations may be written as (T stands for transpose)

$$\mathbf{D} = \varepsilon_0 (\bar{\boldsymbol{\varepsilon}} \cdot \mathbf{E} + Z_0 \bar{\boldsymbol{\kappa}} \cdot \mathbf{H}) \quad (1a)$$

$$\mathbf{B} = \mu_0 \left(-\frac{1}{Z_0} \bar{\boldsymbol{\kappa}}^T \cdot \mathbf{E} + \bar{\boldsymbol{\mu}} \cdot \mathbf{H} \right) \quad (1b)$$

with $Z_0 = \sqrt{\mu_0/\varepsilon_0}$, where $\bar{\boldsymbol{\varepsilon}}$ and $\bar{\boldsymbol{\mu}}$ are the relative electric permittivity and relative magnetic permeability tensors, and $\bar{\boldsymbol{\kappa}}$ is the magneto-electric coupling dimensionless tensor.

Introducing a normalized magnetic field $\mathcal{H} = Z_0 \mathbf{H}$, where k_0 is the free-space wavenumber, from Maxwell's curl equations for source

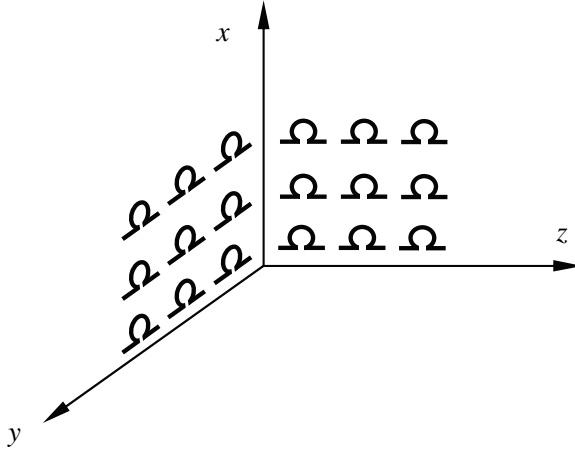


Figure 2. Uniaxial omega medium: coordinate system and spatial orientation of the two identical ensembles of Ω -shaped conducting microstructures in the host isotropic medium.

free regions, together with (1a) and (1b), one may write

$$-j\nabla' \times \mathcal{H} = \bar{\epsilon} \cdot \mathbf{E} + \bar{\kappa} \cdot \mathcal{H} \quad (2a)$$

$$j\nabla' \times \mathbf{E} = -\bar{\kappa}^T \cdot \mathbf{E} + \bar{\mu} \cdot \mathcal{H} \quad (2b)$$

where time-harmonic field variation of the form $\exp(j\omega t)$ was assumed, and $\nabla' = \nabla/k_0$.

Hereafter, for the sake of simplicity of the analysis, we will only consider uniaxial omega media [24]. These media can be built by the inclusion of two stacked sets of identical omega-shaped microstructures in the host medium, but with a different orientation. When the orientation of these two ensembles relative to the coordinate system (x, y, z) is as shown in Fig. 2, the effective medium exhibits a vertical optical axis so that, after a proper homogenization, the constitutive tensors $\bar{\epsilon}$, $\bar{\mu}$ and $\bar{\kappa}$ can be written in the following dyadic form

$$\bar{\epsilon} = \epsilon_{\parallel} \hat{x}\hat{x} + \epsilon_{\perp} (\hat{y}\hat{y} + \hat{z}\hat{z}) \quad (3a)$$

$$\bar{\mu} = \mu_{\parallel} \hat{x}\hat{x} + \mu_{\perp} (\hat{y}\hat{y} + \hat{z}\hat{z}) \quad (3b)$$

$$\bar{\kappa} = j\Omega (\hat{y}\hat{z} - \hat{z}\hat{y}) \quad (3c)$$

where Ω , herein referred as the omega parameter, can be either positive or negative, depending on the orientation of the loops. In the case of a lossless medium, these constitutive parameters are all real.

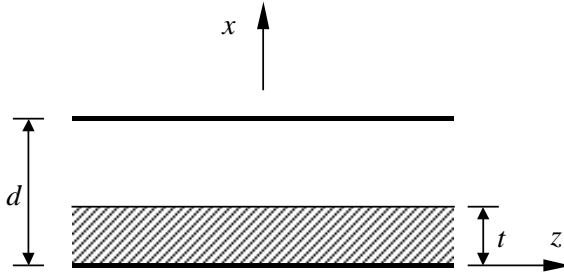


Figure 3. Grounded omega slab with an upper-shielding.

2.2. Field Theory and Modal Equations

In this subsection, we analyze a grounded omega slab with an upper shielding, as depicted in Fig. 3. Let $\eta = t/d$ be the filling factor of the structure, with $0 \leq \eta \leq 1$. Since it is completely closed by perfectly conducting planes placed at $x = 0$ and $x = d$, only discrete modes may propagate.

Introducing normalized variables $x' = k_0x$, $y' = k_0y$ and $z' = k_0z$, and considering plane wave propagation of the form $\exp(-j\beta z')$, where $\beta = k_z/k_0$ is the normalized longitudinal wavenumber, one has $\nabla' = \partial_{x'}\hat{x} - j\beta\hat{z}$, with $\partial_{x'}$ standing for $\partial/\partial x'$. After substituting (3) into (2) and eliminating the components directed along x , one obtains the following set of coupled partial differential equations:

$$\partial_{x'} \mathbf{f}_t = -j\overline{\mathbf{C}} \cdot \mathbf{f}_t, \tag{4}$$

where \mathbf{f}_t is the column vector of the electric and the normalized magnetic field components tangential to the yz plane

$$\mathbf{f}_t = [E_y \quad \mathcal{H}_z \quad \mathcal{H}_y \quad E_z]^T, \tag{5}$$

and $\overline{\mathbf{C}}$ is a coupling matrix given by

$$\overline{\mathbf{C}} = \begin{bmatrix} -j\Omega & \mu_{\perp} & 0 & 0 \\ \varepsilon_{\perp} - \frac{\beta^2}{\mu_{\parallel}} & j\Omega & 0 & 0 \\ 0 & 0 & j\Omega & -\varepsilon_{\perp} \\ 0 & 0 & -\mu_{\perp} + \frac{\beta^2}{\varepsilon_{\parallel}} & -j\Omega \end{bmatrix}. \tag{6}$$

Since $tr\overline{\mathbf{C}} = 0$ and $tr(adj\overline{\mathbf{C}}) = 0$, the four eigenvalues of $\overline{\mathbf{C}}$ are anti-symmetrically paired. Moreover, the field components transverse to

the optical axis are algebraically expressed as $\mathbf{f}_n = \overline{\mathbf{G}} \cdot \mathbf{f}_t$, where

$$\mathbf{f}_n = [\mathcal{H}_x \quad E_x]^T, \quad (7)$$

and $\overline{\mathbf{G}}$ is given by

$$\overline{\mathbf{G}} = \begin{bmatrix} -\frac{\beta}{\mu_{\parallel}} & 0 & 0 & 0 \\ \mu_{\parallel} & & & \\ 0 & 0 & \frac{\beta}{\varepsilon_{\parallel}} & 0 \end{bmatrix}. \quad (8)$$

Since the matrices $\overline{\mathbf{C}}$ and $\overline{\mathbf{G}}$ are block-diagonal, TE and TM modes may propagate in this structure.

For the TE modes, with field components E_y , \mathcal{H}_x and \mathcal{H}_z , using (4) and choosing E_y as the support field component, the Helmholtz equation for E_y can be obtained, with the normalized transverse wavenumber h being given by

$$h^2 = \mu_{\perp} \varepsilon_{\perp} - \Omega^2 - \frac{\mu_{\perp}}{\mu_{\parallel}} \beta^2. \quad (9)$$

The Helmholtz equation and the boundary conditions at $x = 0$ and $x = d$, define a Sturm-Liouville eigenvalue problem [25]. Moreover, introducing the following scalar inner product

$$\langle \phi, \psi \rangle = \int_0^{d'} \phi(x') \psi(x') dx', \quad (10)$$

the orthogonality relation for the TE modes can be easily written as

$$\left\langle \frac{1}{\varepsilon_{\parallel}} E_{y_m}, E_{y_n} \right\rangle = \delta_{mn}, \quad (11)$$

where δ_{mn} represents the Kronecker delta.

In the case of the TM modes, analogous relations can be derived by duality for the field components \mathcal{H}_y , E_x and E_z . Following a similar procedure, the Helmholtz equation for \mathcal{H}_y leads to

$$h^2 = \mu_{\perp} \varepsilon_{\perp} - \Omega^2 - \frac{\varepsilon_{\perp}}{\varepsilon_{\parallel}} \beta^2, \quad (12)$$

while the orthogonality relation can now be written as

$$\left\langle \frac{1}{\mu_{\parallel}} \mathcal{H}_{y_m}, \mathcal{H}_{y_n} \right\rangle = \delta_{mn}. \quad (13)$$

In the TE mode case, enforcing the boundary conditions at $x' = 0$ and $x' = t'$, one gets

$$[\mu_{\perp}q \cot(qa') + \Omega] + h \cot(ht') = 0, \tag{14}$$

which is the modal equation for TE modes. Similarly, for TM modes, one has

$$\left[h^2 + \Omega^2 + \varepsilon_{\perp}q\Omega \tan(qa') \right] + \varepsilon_{\perp}qh \cot(ht') \tan(qa') = 0, \tag{15}$$

which is the modal equation for TM modes. The modes propagating in this structure can be either fast or slow modes, depending on the value of β . In the case of the slow modes, i.e., $\beta > 1$, one has $q = -j\alpha (\alpha > 0)$, with $\alpha^2 = \beta^2 - 1$. Moreover, the fundamental mode of the structure is the TM_0 mode.

The operational diagram of the normalized longitudinal wavenumber β as a function of the filling factor η , for the first TE and TM modes, is shown in Fig. 4, where a structure with $d/\lambda = 2.0$, $\varepsilon_{\parallel} = 2$, $\varepsilon_{\perp} = 3$, $\mu_{\parallel} = 1$, $\mu_{\perp} = 2$ and $\Omega = 0.5$ is considered. For a certain

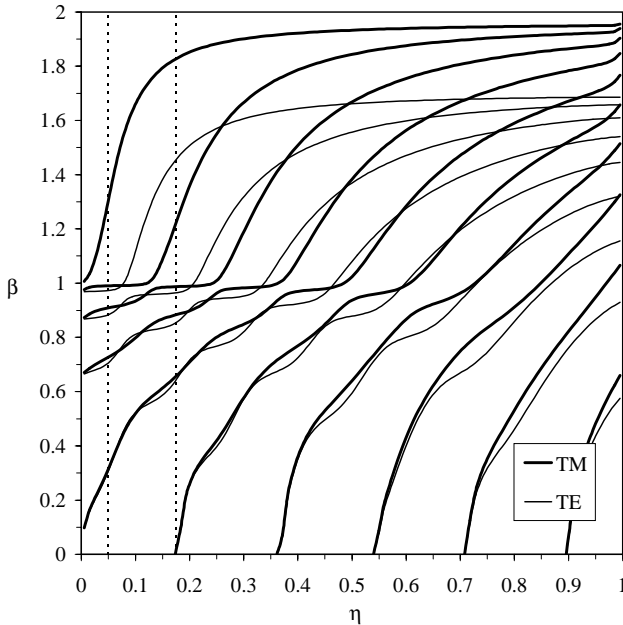


Figure 4. Operational diagram of a partially filled omega parallel-plate waveguide, with $d/\lambda = 2.0$, $\varepsilon_{\parallel} = 2$, $\varepsilon_{\perp} = 3$, $\mu_{\parallel} = 1$, μ_{\perp} and $\Omega = 0.5$.

value of the filling factor η , a vertical line drawn in this diagram allows us to know how many modes are propagating above cutoff and which are the values of their longitudinal wavenumbers. These results are necessary for the next section where the analysis of the omega ridge waveguide is developed.

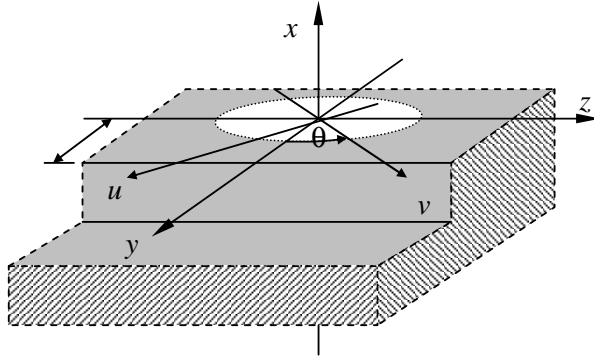


Figure 5. Oblique incidence on the step discontinuity along the v -axis.

3. OMEGA RIDGE WAVEGUIDE

3.1. Analysis of the Step Discontinuity

The starting point for the analysis of the 3D omega ridge waveguide is the study of a step discontinuity under oblique incidence, as shown in Fig. 5. The coordinate system (x, u, v) is used for an incident wave impinging on the discontinuity along the v -axis, at an angle θ with the y -axis. Hence,

$$n_{\text{eff}} - j\alpha = \beta \sin \theta, \quad (16)$$

where n_{eff} is the effective index of refraction of the modes propagating in the 3D omega waveguide and α , with $\alpha > 0$, is its leakage attenuation constant. In (16) β represents the normalized longitudinal wavenumber for either a TE or a TM surface mode. One should note that the constitutive tensors, written in the (x, u, v) coordinate system, take exactly the same form as in (3), just replacing the y and z axes by the u and v axes, respectively.

Oblique incidence couples the elementary TE and TM modes. In fact, after a simple coordinate rotation, these modes become hybrid modes in the structure coordinate system (x, y, z) , where they possess five field components. These hybrid modes are LSE ($E_x = 0$) and LSM modes ($\mathcal{H}_x = 0$) [25].

The scattering matrix of the discontinuity is now derived. This matrix relates the amplitudes of the incident and reflected TE and TM surface modes at $y = w$. It can be obtained by imposing the boundary conditions to the field components tangential to the interface between the two regions.

At the discontinuity $y = w$, every incident, reflected or transmitted field component, must be written as an infinite sum over the fields of all the surface TE and TM modes propagating in the two regions of the structure. Hence, for the LSM modes, one has (I stands for the fields in the thicker region and II for the thinner)

$$\left\{ \begin{array}{l} E_x^i = \frac{1}{\varepsilon_{\parallel}^I(x')} \sum_{n=0}^{\infty} a_{\text{TM}_n} \beta_{\text{TM}_n}^I \phi_{\text{TM}_n}^I(x') \\ E_x^r = \frac{1}{\varepsilon_{\parallel}^I(x')} \sum_{n=0}^{\infty} b_{\text{TM}_n} \beta_{\text{TM}_n}^I \phi_{\text{TM}_n}^I(x') \\ E_x^t = \frac{1}{\varepsilon_{\parallel}^{\text{II}}(x')} \sum_{p=0}^{\infty} c_{\text{TM}_p} \beta_{\text{TM}_p}^{\text{II}} \phi_{\text{TM}_p}^{\text{II}}(x') \end{array} \right. \quad (17)$$

while, for the LSE modes,

$$\left\{ \begin{array}{l} \mathcal{H}_x^i = -\frac{1}{\mu_{\parallel}^I(x')} \sum_{n=1}^{\infty} a_{\text{TE}_n} \beta_{\text{TE}_n}^I \phi_{\text{TE}_n}^I(x') \\ \mathcal{H}_x^r = -\frac{1}{\mu_{\parallel}^I(x')} \sum_{n=1}^{\infty} b_{\text{TE}_n} \beta_{\text{TE}_n}^I \phi_{\text{TE}_n}^I(x') \\ \mathcal{H}_x^t = -\frac{1}{\mu_{\parallel}^{\text{II}}(x')} \sum_{p=1}^{\infty} c_{\text{TE}_p} \beta_{\text{TE}_p}^{\text{II}} \phi_{\text{TE}_p}^{\text{II}}(x') \end{array} \right. , \quad (18)$$

where the factor $\exp\{-j[(n_{\text{eff}} - j\alpha)z' - \omega t]\}$ was omitted. The coefficients a_n , b_n and c_n are the amplitudes of the incident, reflected and transmitted n -order mode, either for TE or TM modes, and ϕ_n its transverse eigenfunction.

Introducing the following vectors

$$\mathbf{a} = \begin{bmatrix} \mathbf{a}_{\text{TE}} \\ \mathbf{a}_{\text{TM}} \end{bmatrix} \quad (19)$$

and

$$\mathbf{b} = \begin{bmatrix} \mathbf{b}_{\text{TE}} \\ \mathbf{b}_{\text{TM}} \end{bmatrix}, \quad (20)$$

where $\mathbf{a}_{\text{TE}} = [a_{\text{TE}_1}, a_{\text{TE}_2}, \dots, a_{\text{TE}_n}, \dots]^T$ is an infinite column vector and similarly for \mathbf{a}_{TM} , \mathbf{b}_{TE} and \mathbf{b}_{TM} , one gets

$$\mathbf{b} = \vec{\Gamma} \cdot \mathbf{a}, \quad (21)$$

where $\vec{\Gamma}$ is the scattering matrix of the discontinuity.

From the continuity of E_x at $y = 0$, one may write

$$\begin{aligned} & \frac{1}{\varepsilon_{\parallel}^{\text{I}}(x')} \sum_{n=0}^{\infty} (a_{\text{TM}_n} + b_{\text{TM}_n}) \beta_{\text{TM}_n}^{\text{I}} \phi_{\text{TM}_n}^{\text{I}}(x') \\ &= -\frac{1}{\mu_{\parallel}^{\text{II}}(x')} \sum_{p=1}^{\infty} c_{\text{TE}_p} \beta_{\text{TE}_p}^{\text{II}} \phi_{\text{TE}_p}^{\text{II}}(x'), \end{aligned} \quad (22)$$

while, from the continuity of \mathcal{H}_x , one obtains

$$\begin{aligned} & -\frac{1}{\mu_{\parallel}^{\text{I}}(x')} \sum_{n=1}^{\infty} (a_{\text{TE}_n} + b_{\text{TE}_n}) \beta_{\text{TE}_n}^{\text{I}} \phi_{\text{TE}_n}^{\text{I}}(x') \\ &= -\frac{1}{\mu_{\parallel}^{\text{II}}(x')} \sum_{p=1}^{\infty} c_{\text{TE}_p} \beta_{\text{TE}_p}^{\text{II}} \phi_{\text{TE}_p}^{\text{II}}(x'). \end{aligned} \quad (23)$$

On the other hand, imposing the continuity of E_z at $y = 0$, one may write

$$\begin{aligned} & -\sum_{n=1}^{\infty} (a_{\text{TE}_n} - b_{\text{TE}_n}) \cos \theta_{\text{TE}_n}^{\text{I}} \phi_{\text{TE}_n}^{\text{I}}(x') \\ & -j \frac{1}{\varepsilon_{\perp}^{\text{I}}(x')} \sum_{n=0}^{\infty} (a_{\text{TM}_n} + b_{\text{TM}_n}) \sin \theta_{\text{TM}_n}^{\text{I}} \left[\partial_{x'} \phi_{\text{TM}_n}^{\text{I}} - \Omega^{\text{I}}(x') \phi_{\text{TM}_n}^{\text{I}}(x') \right] \\ &= -\sum_{p=1}^{\infty} c_{\text{TE}_p} \cos \theta_{\text{TE}_p}^{\text{II}} \phi_{\text{TE}_p}^{\text{II}}(x') \\ & -j \frac{1}{\varepsilon_{\perp}^{\text{II}}(x')} \sum_{p=0}^{\infty} c_{\text{TM}_p} \sin \theta_{\text{TM}_p}^{\text{II}} \left[\partial_{x'} \phi_{\text{TM}_p}^{\text{II}} - \Omega^{\text{II}}(x') \phi_{\text{TM}_p}^{\text{II}}(x') \right] \end{aligned} \quad (24)$$

while the continuity of \mathcal{H}_z leads to

$$\begin{aligned} & j \frac{1}{\mu_{\perp}^{\text{I}}(x')} \sum_{n=1}^{\infty} (a_{\text{TE}_n} + b_{\text{TE}_n}) \sin \theta_{\text{TE}_n}^{\text{I}} \left[\partial_{x'} \phi_{\text{TE}_n}^{\text{I}} + \Omega^{\text{I}}(x') \phi_{\text{TE}_n}^{\text{I}}(x') \right] \\ & - \sum_{n=0}^{\infty} (a_{\text{TM}_n} - b_{\text{TM}_n}) \cos \theta_{\text{TM}_n}^{\text{I}} \phi_{\text{TM}_n}^{\text{I}}(x') \end{aligned}$$

$$\begin{aligned}
 &= j \frac{1}{\mu_{\perp}^{\text{II}}(x')} \sum_{p=1}^{\infty} c_{\text{TE}_p} \cos \theta_{\text{TE}_p}^{\text{II}} \left[\partial_{x'} \phi_{\text{TE}_p}^{\text{II}} + \Omega^{\text{II}}(x') \phi_{\text{TE}_p}^{\text{II}}(x') \right] \\
 &\quad - \sum_{p=0}^{\infty} c_{\text{TM}_p} \cos \theta_{\text{TM}_p}^{\text{II}} \phi_{\text{TM}_p}^{\text{II}}(x').
 \end{aligned} \tag{25}$$

In the following, a conventional mode-matching technique is applied. After multiplying (22) by $\phi_{\text{TM}_m}^{\text{II}}$ and (23) by $\phi_{\text{TE}_m}^{\text{II}}$, integrating between 0 and d' , and using the orthogonality relations (13) and (11), respectively, the expressions for c_{TM_m} and c_{TE_m} are derived. Using this result, multiplying (24) by $\phi_{\text{TE}_m}^{\text{II}}/\mu_{\parallel}^{\text{II}}$ and (25) by $\phi_{\text{TM}_m}^{\text{II}}/\varepsilon_{\parallel}^{\text{II}}$, integrating and using again the orthogonality relations, one may finally derive the following matrix system

$$\overline{\mathbf{A}} \cdot \mathbf{a} = \overline{\mathbf{B}} \cdot \mathbf{b}, \tag{26}$$

where

$$\overline{\mathbf{A}} = \begin{bmatrix} \overline{\mathbf{A}}^{11} & \overline{\mathbf{A}}^{12} \\ \overline{\mathbf{A}}^{21} & \overline{\mathbf{A}}^{22} \end{bmatrix} \tag{27}$$

and

$$\overline{\mathbf{B}} = \begin{bmatrix} \overline{\mathbf{B}}^{11} & \overline{\mathbf{B}}^{12} \\ \overline{\mathbf{B}}^{21} & \overline{\mathbf{B}}^{22} \end{bmatrix}, \tag{28}$$

with

$$A_{mn}^{11} = \cos \theta_{\text{TE}_n}^{\text{I}} R_{mn} - \frac{\cos \theta_{\text{TE}_m}^{\text{II}}}{\beta_{\text{TE}_m}^{\text{II}}} \beta_{\text{TE}_n}^{\text{I}} Q_{mn} \tag{29a}$$

$$A_{mn}^{12} = j \left(\sin \theta_{\text{TM}_n}^{\text{I}} S_{mn} - \beta_{\text{TM}_n}^{\text{I}} \sum_{p=1}^{\infty} \frac{\sin \theta_{\text{TM}_p}^{\text{II}}}{\beta_{\text{TM}_p}^{\text{II}}} P_{pn} T_{mp} \right) \tag{29b}$$

$$A_{mn}^{21} = j \left(\sin \theta_{\text{TE}_n}^{\text{I}} U_{mn} - \beta_{\text{TE}_n}^{\text{I}} \sum_{p=1}^{\infty} \frac{\sin \theta_{\text{TE}_p}^{\text{II}}}{\beta_{\text{TE}_p}^{\text{II}}} Q_{pn} X_{mp} \right) \tag{29c}$$

$$A_{mn}^{22} = -\cos \theta_{\text{TM}_n}^{\text{I}} V_{mn} + \frac{\cos \theta_{\text{TM}_m}^{\text{II}}}{\beta_{\text{TM}_m}^{\text{II}}} \beta_{\text{TM}_n}^{\text{I}} P_{mn} \tag{29d}$$

and

$$B_{mn}^{11} = \cos \theta_{\text{TE}_n}^{\text{I}} R_{mn} + \frac{\cos \theta_{\text{TE}_m}^{\text{II}}}{\beta_{\text{TE}_m}^{\text{II}}} \beta_{\text{TE}_n}^{\text{I}} Q_{mn} \tag{30a}$$

$$B_{mn}^{12} = -A_{mn}^{12} \tag{30b}$$

$$B_{mn}^{21} = -A_{mn}^{21} \quad (30c)$$

$$B_{mn}^{22} = -\cos \theta_{\text{TM}_n}^{\text{I}} V_{mn} - \frac{\cos \theta_{\text{TM}_m}^{\text{II}}}{\beta_{\text{TM}_m}^{\text{II}}} \beta_{\text{TM}_n}^{\text{I}} P_{mn}. \quad (30d)$$

The following inner products have been introduced

$$P_{mn} = \left\langle \frac{1}{\varepsilon_{\parallel}^{\text{I}}} \phi_{\text{TM}_n}^{\text{I}}, \phi_{\text{TM}_m}^{\text{II}} \right\rangle \quad (31a)$$

$$Q_{mn} = \left\langle \frac{1}{\mu_{\parallel}^{\text{I}}} \phi_{\text{TE}_n}^{\text{I}}, \phi_{\text{TE}_m}^{\text{II}} \right\rangle \quad (31b)$$

$$R_{mn} = \left\langle \phi_{\text{TE}_n}^{\text{I}}, \frac{1}{\mu_{\parallel}^{\text{II}}} \phi_{\text{TE}_m}^{\text{II}} \right\rangle \quad (31c)$$

$$S_{mn} = \left\langle \frac{1}{\varepsilon_{\perp}^{\text{I}}} \left(\partial_{x'} \phi_{\text{TM}_n}^{\text{I}} - \Omega^{\text{I}} \phi_{\text{TM}_n}^{\text{I}} \right), \frac{1}{\mu_{\parallel}^{\text{II}}} \phi_{\text{TE}_m}^{\text{II}} \right\rangle \quad (31d)$$

$$T_{mp} = \left\langle \frac{1}{\varepsilon_{\perp}^{\text{II}}} \left(\partial_{x'} \phi_{\text{TM}_p}^{\text{II}} - \Omega^{\text{II}} \phi_{\text{TM}_p}^{\text{II}} \right), \frac{1}{\mu_{\parallel}^{\text{II}}} \phi_{\text{TE}_m}^{\text{II}} \right\rangle \quad (31e)$$

$$U_{mn} = \left\langle \frac{1}{\mu_{\perp}^{\text{I}}} \left(\partial_{x'} \phi_{\text{TE}_n}^{\text{I}} + \Omega^{\text{I}} \phi_{\text{TE}_n}^{\text{I}} \right), \frac{1}{\varepsilon_{\parallel}^{\text{II}}} \phi_{\text{TM}_m}^{\text{II}} \right\rangle \quad (31f)$$

$$V_{mn} = \left\langle \phi_{\text{TM}_n}^{\text{I}}, \frac{1}{\varepsilon_{\parallel}^{\text{II}}} \phi_{\text{TM}_m}^{\text{II}} \right\rangle \quad (31g)$$

$$X_{mp} = \left\langle \frac{1}{\mu_{\perp}^{\text{II}}} \left(\partial_{x'} \phi_{\text{TE}_n}^{\text{II}} + \Omega^{\text{II}} \phi_{\text{TE}_n}^{\text{II}} \right), \frac{1}{\varepsilon_{\parallel}^{\text{II}}} \phi_{\text{TM}_p}^{\text{II}} \right\rangle. \quad (31h)$$

Comparing (26) with (21), it is easy to see that $\vec{\Gamma} = \overline{\mathbf{B}}^{-1} \cdot \overline{\mathbf{A}}$. However, $\overline{\mathbf{B}}^{-1}$ can only be computed if $\overline{\mathbf{B}}$ is a finite square matrix. Let N_{TE}^{I} and $N_{\text{TE}}^{\text{II}}$ be the number of TE modes considered, after truncation, in regions I and II, respectively, and N_{TM}^{I} and $N_{\text{TM}}^{\text{II}}$ the same for TM modes. Therefore, one must have $N_{\text{TE}}^{\text{I}} + N_{\text{TM}}^{\text{I}} = N_{\text{TE}}^{\text{II}} + N_{\text{TM}}^{\text{II}}$, i.e., the total number of modes considered in each region must be equal.

3.2. Modal Equation of the 3D Waveguide

Since the scattering matrix of the step discontinuity has been derived, now we have the appropriate tools to derive the modal equation of the 3D waveguide. The plane $y = 0$ is a symmetry plane. In fact, relatively to this plane, the propagating modes can be divided into even and odd

modes. For the even modes the symmetry plane can be replaced by an electric plane while, for the odd modes, a magnetic plane can replace it.

In the case of the even modes, the longitudinal components of the magnetic field vanish in this plane, i.e.,

$$\mathcal{H}_x^i + \mathcal{H}_x^r = 0 \quad (32a)$$

$$\mathcal{H}_z^i + \mathcal{H}_z^r = 0, \quad (32b)$$

while, for the odd modes,

$$E_x^i + E_x^r = 0 \quad (33a)$$

$$E_z^i + E_z^r = 0. \quad (33b)$$

From (32a) and (32b) one may write

$$\overline{\mathbf{W}}_{\text{TE}}^{-1} \cdot \mathbf{a}_{\text{TE}} = -\overline{\mathbf{W}}_{\text{TE}} \cdot \mathbf{b}_{\text{TE}} \quad (34a)$$

$$\overline{\mathbf{W}}_{\text{TM}}^{-1} \cdot \mathbf{a}_{\text{TM}} = \overline{\mathbf{W}}_{\text{TM}} \cdot \mathbf{b}_{\text{TM}} \quad (34b)$$

where

$$\overline{\mathbf{W}}_{\text{TE}} = \text{diag} \left(e^{-j\beta_{\text{TE}1}^I \cos \theta_{\text{TE}1}^I w'}, e^{-j\beta_{\text{TE}2}^I \cos \theta_{\text{TE}2}^I w'}, \dots \right) \quad (35a)$$

$$\overline{\mathbf{W}}_{\text{TM}} = \text{diag} \left(e^{-j\beta_{\text{TM}0}^I \cos \theta_{\text{TM}0}^I w'}, e^{-j\beta_{\text{TM}1}^I \cos \theta_{\text{TM}1}^I w'}, \dots \right) \quad (35b)$$

On the other hand, from (33a) and (33b), one has

$$\overline{\mathbf{W}}_{\text{TE}}^{-1} \cdot \mathbf{a}_{\text{TE}} = \overline{\mathbf{W}}_{\text{TE}} \cdot \mathbf{b}_{\text{TE}} \quad (36a)$$

$$\overline{\mathbf{W}}_{\text{TM}}^{-1} \cdot \mathbf{a}_{\text{TM}} = -\overline{\mathbf{W}}_{\text{TM}} \cdot \mathbf{b}_{\text{TM}}. \quad (36b)$$

Therefore, setting $\Gamma = 1$ for even modes and $\Gamma = -1$ for odd modes, one gets

$$\vec{\Gamma} = \Gamma \overline{\boldsymbol{\sigma}} \cdot \overline{\mathbf{W}}, \quad (37)$$

with

$$\overline{\boldsymbol{\sigma}} = \text{diag}(-1, -1, \dots, +1, +1, \dots) \quad (38)$$

and

$$\overline{\mathbf{W}} = \text{diag} \left(\overline{\mathbf{W}}_{\text{TE}}^2, \overline{\mathbf{W}}_{\text{TM}}^2 \right), \quad (39)$$

and the following equation can be derived

$$\mathbf{a} = \vec{\Gamma} \cdot \mathbf{b}. \quad (40)$$

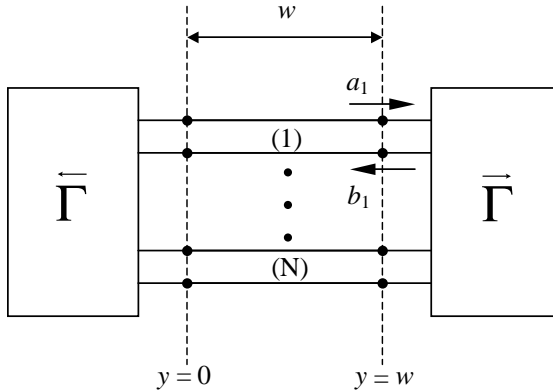


Figure 6. Equivalent network for the 3D waveguide.

The equivalent network for the 3D waveguide is depicted in Fig. 6. From (40) together with (21), one may finally write

$$(\bar{\mathbf{I}} - \vec{\mathbf{\Gamma}} \cdot \vec{\mathbf{\Gamma}}) \cdot \mathbf{a} = \mathbf{0}, \quad (41)$$

where $\bar{\mathbf{I}}$ is the identity matrix. A non-trivial solution for (41), implies that

$$\det(\bar{\mathbf{I}} - \vec{\mathbf{\Gamma}} \cdot \vec{\mathbf{\Gamma}}) = 0, \quad (42)$$

which is the modal equation of the 3D omega waveguide.

4. NUMERICAL RESULTS

In this section, some numerical results for the upper-shielded omega ridge waveguide shown in Fig. 7, are presented. These results have been obtained including all the elementary surface modes propagating above cutoff in each region.

Let $\zeta = t^{\text{II}}/t^{\text{I}}$, with $0 \leq \zeta \leq 1$, be the step size and $\xi = w/d$, with $0 \leq \xi < \infty$, be the waveguide aspect ratio. In this example, we have considered $t^{\text{I}}/\lambda = 0.35$, $\Omega = 0.5$, and $\zeta = 0.35$ while, for the other constitutive parameters, we have kept the same values as used in Section 2. Two values of η are considered: $\eta^{\text{I}} = 0.175$ and $\eta^{\text{II}} = 0.05$. One should note that these values of η guarantee that the position of the upper-shielding does not affect the numerical values of the propagation constants. Therefore, these results are valid for the open structure.

With these numerical data, the elementary modes propagating in the inner and outer regions correspond exactly to those modes

Table 1. Normalized longitudinal wavenumbers for the first guided modes.

		TM ₀		TE ₁	
η^I	0.175	$\beta_{TM_0}^I$	1.828	$\beta_{TE_1}^I$	1.456
η^{II}	0.05	$\beta_{TM_0}^{II}$	1.307	$\beta_{TE_1}^{II}$	0.973

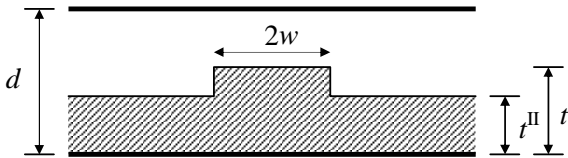


Figure 7. Omega ridge waveguide with an upper shielding.

intersected by the vertical dashed lines drawn on Fig. 4. For any of these values there are, at least, four pairs of TE and TM modes propagating above cutoff, which have been included in the calculations.

The values of the normalized longitudinal wavenumbers of the first and second propagating modes, listed in Table 1, are important to determine the critical angles for total internal reflection in the inner region. These angles are related with the asymptotic and cutoff values of the effective refractive index of the modes in the ridge waveguide, which will be presented in Fig. 9 and Fig. 10.

The operational diagram for the first guided modes propagating in the omega ridge waveguide, is shown in Fig. 8. These curves were all calculated for $n_{\text{eff}} = \beta_{TM_0}^{II}$. Hereafter, the modes are termed as H_n meaning that they are all hybrid, where n is the order of the mode expressing the number of maximums in the inner region. There is a fundamental mode with no cutoff, as expected.

The effective index of refraction n_{eff} of the modes in the ridge waveguide is shown in Fig. 9 as a function of the aspect ratio ξ , for the first even and odd guided modes. Mode coupling between some of the curves can be easily identified. As was already pointed out, due to the waveguide spatial symmetry relatively to the central plane $y = 0$, every propagating mode has either even or odd symmetry. Therefore, hybrid mode coupling is only possible among the modes with the same parity while curves displaying different parity modes crossover each other.

For the same waveguide and with identical numerical parameters,

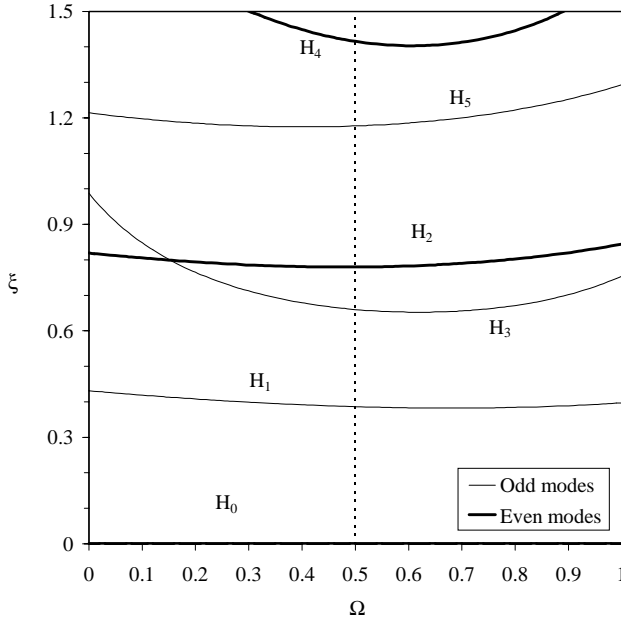


Figure 8. Operational diagram of an omega ridge waveguide with $d/\lambda = 2.0$, $t^I/\lambda = 0.35$ and $\zeta = 0.35$.

Fig. 10 shows the operational diagram of the first leaky modes propagating below cutoff. The thicker part of the dispersion curves corresponds to the range where the mode becomes effectively a leaky mode. Leakage will only occur as long as one of the elementary surface modes propagating in the outer region ceases to be totally reflected at the step discontinuities. One should note that some modes never turn into proper leaky modes. Moreover, mode H_2 is the first mode suffering power leakage, since the fundamental mode H_0 and mode H_1 never become leaky.

The root locus in the complex plane of the normalized longitudinal wavenumber, for the first leaky mode H_2 , is shown in Fig. 11. We can easily see that the peak value for the leakage constant increases monotonically with the value of the Ω parameter (in the limit $\Omega = 0$ corresponds to the common uniaxial anisotropic case), while the peak width decreases.

The attenuation constant due to the leakage effect, in dB/ λ , as a function of ξ , for the same leaky mode, is depicted in Fig. 12. It can be concluded that an increase in the omega parameter is responsible for a higher leakage loss in a wider band of ξ values. Moreover, as already

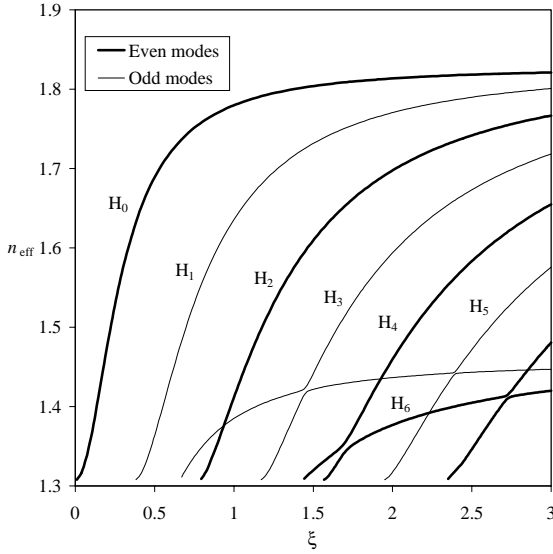


Figure 9. Operational diagram of an omega ridge waveguide with $d/\lambda = 2.0$, $t^I/\lambda = 0.35$, $\Omega = 0.5$ and $\zeta = 0.35$.

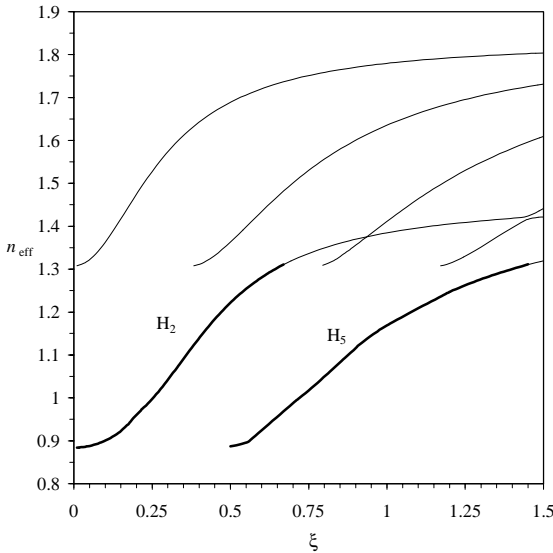


Figure 10. Operational diagram for the first leaky modes propagating in an omega ridge waveguide with $d/\lambda = 2.0$, $t^I/\lambda = 0.35$, $\Omega = 0.5$ and $\zeta = 0.35$.

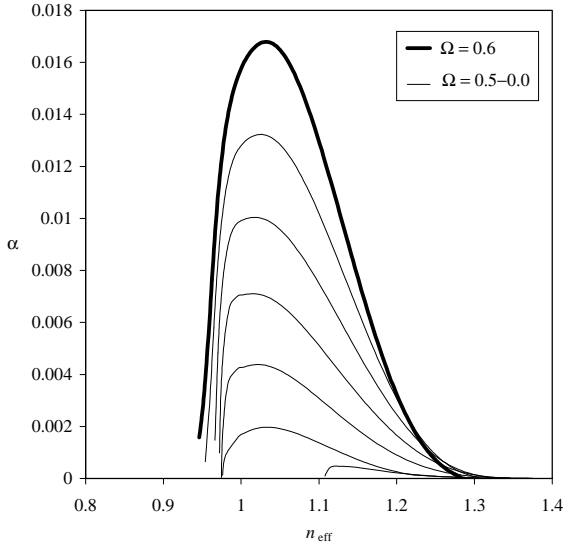


Figure 11. Root locus in the complex plane of the normalized longitudinal wavenumber, for H_2 leaky mode.

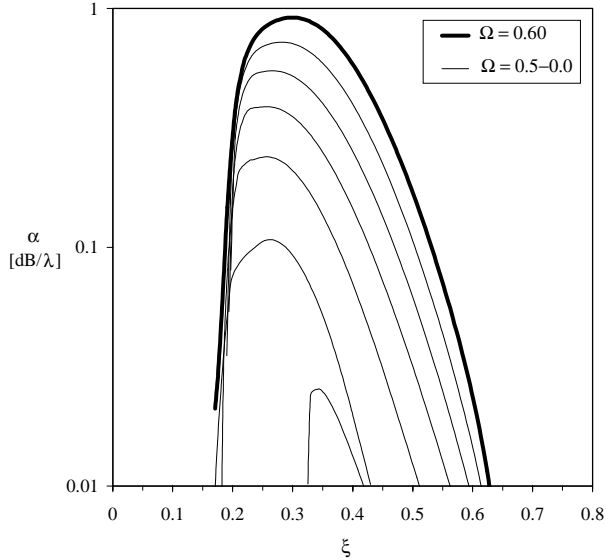


Figure 12. Variation of the attenuation constant, in dB/λ , with the aspect ratio of the ridge waveguide for the leaky mode depicted in Fig. 11.

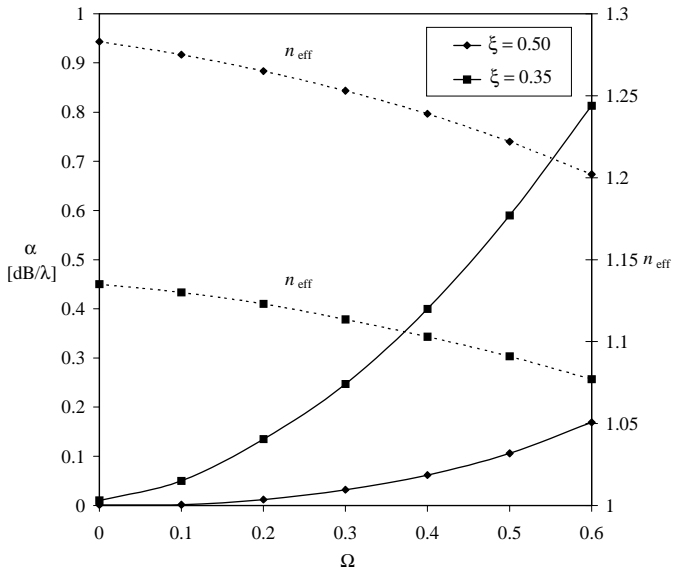


Figure 13. Variation of the leakage and phase constants with Ω , for two values of the aspect ratio ξ .

described in the literature for an isotropic structure, a transverse resonance phenomenon is observed, leading to a periodic cancellation of the leakage effect with a variable strip width [22].

Finally, Fig. 13 shows the leakage and the phase constants of the H_2 leaky mode, as a function of the omega parameter, for two values of ξ .

To check the numerical results presented in this paper, a comparison with the limit isotropic case ($\Omega = 0$) has been done, using the results published by Oliner et al. [22] for the same mode, H_3 in our notation. A dielectric ridge waveguide made with an isotropic medium with $\epsilon = 12$ and $\mu = 1$, and having $t^I/\lambda = 0.2$ and $t^{II}/\lambda = 0.1$, was considered. For the sake of comparison, an isotropic-like omega medium, in the sense that $\epsilon = (2\epsilon_{\perp} + \epsilon_{\parallel})/3$ and $\mu = (2\mu_{\perp} + \mu_{\parallel})/3$, was assumed. In this case, whenever Ω vanishes, a true isotropic (and not uniaxial anisotropic) medium is obtained. In fact, as shown in Fig. 14 for $\Omega = 0$, our results perfectly match those presented in Fig. 15 of [22].

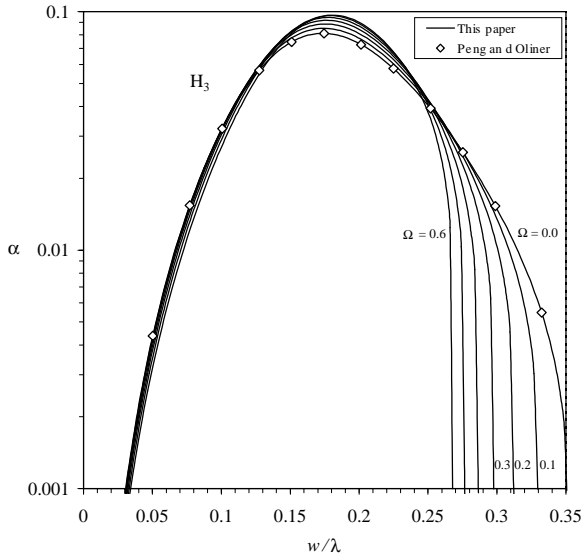


Figure 14. Variation of the leakage constant with w/λ , for several values of Ω . For $\Omega = 0$, our results match those of [22].

5. CONCLUSION

Electromagnetic wave propagation in 3D planar omega waveguides has been addressed in this paper. It was shown that discrete complex hybrid modes can propagate in these structures and results for an omega ridge waveguide were presented, showing the effect of the omega and the geometrical parameters on the leakage behavior of the structure.

ACKNOWLEDGMENT

This work was supported by Fundação para a Ciência e a Tecnologia (FCT) under Project POSI/CPS/39589/2001.

REFERENCES

1. Saadoun, M. M. I. and N. Engheta, "A reciprocal phase shifter using novel pseudochiral or omega medium," *Microwave Opt. Technol. Lett.*, Vol. 5, 184–188, 1992.
2. Jaggard, D. L., A. R. Mickelson, and C. H. Papas, "On

- electromagnetic waves in chiral media,” *Appl. Phys.*, Vol. 18, 211–216, 1979.
3. Yatsenko, V. V., S. I. Maslovski, S. A. Tretyakov, S. L. Prosvirnin, and S. Zoudhi, “Plane-wave reflection from double arrays of small magnetoelectric scatterers,” *IEEE Trans. Antennas and Propagation*, Vol. 51, 2–11, 2003.
 4. Wenyan, Y. and W. Wengbing, “Reflection and transmission for planar structures of uniaxial chiro-omega media,” *Microwave Opt. Technol. Lett.*, Vol. 7, 475–478, 1994.
 5. Yin, W. Y., B. Guo, and X. T. Dong, “Comparative study on the interaction of electromagnetic waves with multi-layer omega(chiro) ferrite slabs,” *J. Electromagn. Waves Appl.*, Vol. 17, 15–29, 2003.
 6. Toscano, A. and L. Vegni, “Novel characteristics of radiation patterns of a pseudochiral point-source antenna,” *Microwave Opt. Technol. Lett.*, Vol. 7, 247–250, 1994.
 7. Norgren, M. and S. He, “Reconstruction of the constitutive parameters for an omega material in a rectangular waveguide,” *IEEE Trans. Microwave Theory Tech.*, Vol. 43, 1315–1321, 1995.
 8. Dorko, K. and J. Mazur, “Characterization of rectangular waveguide with a pseudochiral omega slab,” *IEEE Microwave Wireless Component Lett.*, Vol. 12, 482–484, 2002.
 9. Wenyan, Y., W. Wei, and S. Xiaowei, “Mode characteristics in a lossy parallel-plate uniaxial chiro-omega waveguide,” *Microwave Opt. Technol. Lett.*, Vol. 7, 868–870, 1994.
 10. Wenyan, Y., W. Wei, and W. Wenbing, “Mode characteristics in a circular uniaxial chiro-omega waveguide,” *Electron. Letters*, Vol. 30, 1072–1074, 1994.
 11. Mazur, J. and D. Pietrzak, “Field displacement phenomenon in a rectangular waveguide containing a thin plate of omega medium,” *IEEE Microwave Guided Wave Lett.*, Vol. 6, 34–36, 1996.
 12. Topa, A. L., C. R. Paiva, and A. M. Barbosa, “Propagation characteristics of the rectangular waveguide inhomogeneously filled with uniaxial omega media,” *IEICE Trans. Electron.*, Vol. E82-C, 1166–1171, 1999.
 13. Toscano, A. and L. Vegni, “Characteristics of propagation of waveguides filled with an omega medium,” *Proceedings of JINA94*, 50–53, Nice, France, September 1994.
 14. Topa, A. L., C. R. Paiva, and A. M. Barbosa, “Full-wave analysis of a nonradiative dielectric waveguide with a pseudochiral omega slab,” *IEEE Trans. Microwave Theory Tech.*, Vol. 46, 1263–1269, 1998.

15. Saadoun, M. M. I. and N. Engheta, "Pseudochiral omega medium and guided-wave structures: Theory and principles," *Proceedings of the 14th URSI Int. Symp. Electr. Theory*, 302–304, Sydney, Australia, August 1992.
16. Tretyakov, S., "Thin pseudochiral layers: approximate boundary conditions and potential applications," *Microwave Opt. Technol. Lett.*, Vol. 6, 112–115, 1993.
17. Topa, A. L., C. R. Paiva, and A. M. Barbosa, "Complete spectral representation for the electromagnetic field of planar multilayered waveguides containing pseudochiral Ω -media," *Progress In Electromagnetic Research*, J. A. Kong (ed.), PIER 9, Ch. 5, 85–104, EMW Publishing, Cambridge, MA, 1998.
18. Topa, A. L., C. R. Paiva, and A. M. Barbosa, "Surface and leaky modes of multilayered omega structures," *Advances in Electromagnetics of Complex Media and Metamaterials*, Saïd Zouhdi, Ari Sihvola, and Mohamed Arsalane (eds.), 291–306, Kluwer Academic, Dordrecht, 2003.
19. Topa, A. L., C. R. Paiva, and A. M. Barbosa, "Discrete complex spectrum of 3D open omega waveguides," *Abstract in Digest of 2003 URSI/USNC National Radio Science Meeting*, Columbus, Ohio, Vol. 1, 221, June 2003.
20. Topa, A. L., C. R. Paiva, and A. M. Barbosa, "Least squares boundary residual method for the analysis of step discontinuities in open chiral waveguides," *Int. J. Electron. Commun. (AËU)*, Vol. 55, 281–291, 2001.
21. Peng, S.-T. and A. A. Oliner, "Guidance and leakage properties of a class of open dielectric waveguides: Part I — Mathematical formulations," *IEEE Trans. Microwave Theory Tech.*, Vol. MTT-29, 843–855, 1981.
22. Oliner, A. A., S.-T. Peng, T.-H. Hsu, and A. Sanchez, "Guidance and leakage properties of a class of open dielectric waveguides: Part II — New physical effects," *IEEE Trans. Microwave Theory Tech.*, Vol. MTT-29, 855–869, 1981.
23. Serdyukov, V., I. Semchenko, S. Tretyakov, and A. Sihvola, *Electromagnetics of Bi-anisotropic Materials — Theory and Applications*, Ch. 1, Gordon and Breach Science Publishers, Amsterdam, 2001.
24. Tretyakov, S. A., "Uniaxial omega medium as a physically realizable alternative for the perfectly matched layer (PML)," *J. Electromagn. Waves Applic.*, Vol. 12, 821–837, 1998.
25. Collin, R. E., *Field Theory of Guided Waves*, 233–234, McGraw-Hill Book Company, New York, 1960.

Antonio L. Topa was born in Lisbon, Portugal, in 1962. He received the *Licenciado*, Master and Ph.D. degrees in Electrical Engineering from Instituto Superior Técnico (IST) — Technical University of Lisbon, Portugal — in 1985, 1989 and 1998, respectively. He is currently an Assistant Professor at the Department of Electrical and Computer Engineering of IST. He is also a researcher at the Instituto de Telecomunicações (IT), Lisbon. His research interests are in electromagnetic wave propagation in planar structures containing metamaterials and complex media, namely chiral and omega media, and its applications to microwave and integrated optics, as well as to fiber optics.

Carlos R. Paiva was born in Lisbon, Portugal, in 1957. He received the *Licenciado*, Master and Ph.D. degrees in Electrical Engineering from Instituto Superior Técnico (IST) — Technical University of Lisbon, Portugal — in 1982, 1986 and 1992, respectively. He is currently an Associate Professor at the Department of Electrical and Computer Engineering of IST. He is also a researcher at the Instituto de Telecomunicações (IT), Lisbon. His research interests are in photonics, the foundations of classical electrodynamics, the electromagnetic theory of complex media, relativity, quantum physics, differential forms and geometric algebra.

Afonso M. Barbosa was born in Coimbra, Portugal, in 1950. He received the *Licenciado* degree in Electrical Engineering from Instituto Superior Técnico (IST) — Technical University of Lisbon, Portugal, in 1972, the Master degree in electronic engineering from NUFFIC, The Netherlands, in 1974, and the Ph.D. degree in electrical engineering from IST in 1984. He is currently a Full Professor and Head of the Department of Electrical and Computer Engineering of IST, and a researcher at Instituto de Telecomunicações (IT), Lisbon. His research interests are in electromagnetic wave theory and applications, namely microwave, millimeter-wave, and optical waveguide structures, antennas, and scattering with emphasis on complex media.